Chemical Engineering Journal 382 (2020) 122732

Contents lists available at ScienceDirect

Chemical Engineering Journal

journal homepage: www.elsevier.com/locate/cej

Selective photocatalytic oxidation of cyclohexanol to cyclohexanone: A spectroscopic and kinetic study

M.R. Karimi Estahbanati[a], Mehrzad Feilizadeh[b], Alexandre Babin[a], Bastian Mei[c], Guido Mul[c,*], Maria C. Iliuta[a,*]

[a] Department of Chemical Engineering, 1065 Av. De la Médecine, Université Laval, Québec, Québec G1V 0A6, Canada
[b] School of Chemical and Petroleum Engineering, Shiraz University, Shiraz, Iran
[c] PhotoCatalytic Synthesis Group, Faculty of Science & Technology of the University of Twente, PO Box 217, Enschede, The Netherlands

HIGHLIGHTS

- Photocatalytic oxidation of cyclohexanol to cyclohexanone was studied.
- Cyclohexanol transformation was explored by *in situ* ATR-FTIR analysis.
- A reaction mechanism for cyclohexanone production was proposed.
- A kinetic model was developed and validated by current experimental data.
- Cyclohexanol can be selectively converted to cyclohexanone.

GRAPHICAL ABSTRACT

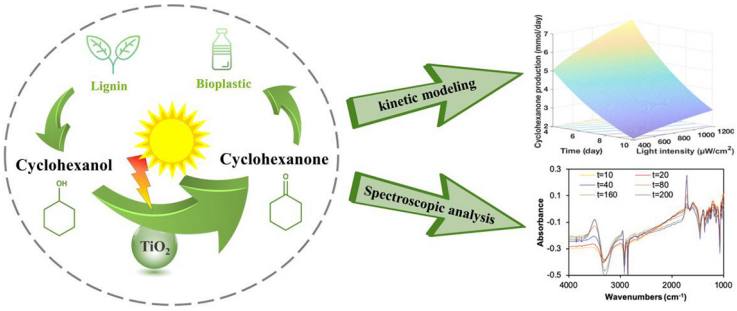

ARTICLE INFO

Keywords:
Photocatalysis
Cyclohexanone
ATR-FTIR
Kinetic model
Spectroscopy

ABSTRACT

In this work, spectroscopic and kinetic studies were performed on photocatalytic oxidation of cyclohexanol to cyclohexanone. The photocatalytic experiments were performed according to a three-level full factorial design and the rate of cyclohexanone production was determined by HPLC analysis. *In situ* ATR-FTIR analysis of the photocatalytic reaction revealed that cyclohexanol can be selectively converted to cyclohexanone, without the formation of significant amounts of carbonates and carboxylates. A reaction mechanism based on different steps from charge separation to cyclohexanone molecule formation is proposed. The results were utilized to determine the kinetic parameters (with the help of genetic algorithm) and validate the model. The developed kinetic model illustrates that the rate of cyclohexanone production increases as a power function with respect to the light intensity and decreases as an exponential function with respect to time. An excellent selectivity of cyclohexanone was confirmed by spectroscopic and chromatographic studies. This study demonstrates that photocatalysis can be a promising technology for formation of cyclohexanone from cyclohexanol.

1. Introduction

In the recent years, great attention has been paid to photocatalytic conversion of chemicals for the purpose of their elimination [1–6] or as a smart approach of synthesis [7–12]. In principle, photocatalytic synthesis can lead to higher selectivity in comparison to conventional oxidation processes [13,14]. As photocatalytic processes operate at moderate conditions, photocatalytic synthesis of temperature or pressure sensitive products is a particular point of interest.

Caprolactam is an important monomer feedstock for nylon-6

* Corresponding authors.
E-mail addresses: g.mul@utwente.nl (G. Mul), maria-cornelia.iliuta@gch.ulaval.ca (M.C. Iliuta).

https://doi.org/10.1016/j.cej.2019.122732
Received 24 June 2019; Received in revised form 30 August 2019; Accepted 4 September 2019
Available online 06 September 2019
1385-8947/

production and it is estimated that around 90% of caprolactam is produced from cyclohexanone [15]. In addition to caprolactam, cyclohexanol is used for production of adipic acid (for nylon-6,6 production) or as solvent for resins, lacquers, dyes, and insecticides [16]. Production of caprolactam requires high temperatures and elevated pressures implying high energy consumption [17]. As cyclohexanol can be sustainably produced from lignin [18], the photocatalytic production of cyclohexanone from cyclohexanol and subsequent conversion to caprolactam can be a sustainable approach for the production of nylon-6 [19].

In our previous work on photocatalytic production of cyclohexanone from cyclohexane, a mixture of cyclohexanone and cyclohexanol was detected as final product [20]. It was revealed that strongly adsorbed intermediates further oxidize to carboxylates and cause catalyst deactivation [21]. The selectivity to cyclohexanone is a key factor in the transformation of cyclohexanol [22–24]. A higher cyclohexanone purity increases the process efficiency by reducing energy consumption [25].

In this context, our aim was to explore the possibility to produce cyclohexanone from cyclohexanol with high selectivity, and to minimize catalyst deactivation as caused by carboxylate formation. In particular, a mechanistic and kinetic study was performed on the photocatalytic production of cyclohexanone from cyclohexanol using a TiO_2-based photocatalyst. In this regard, an *in situ* ATR–FTIR (attenuated total reflectance–Fourier transform infrared) analysis was employed, as a feasible technique for real time mechanistic understanding of the photocatalytic reaction and analysis of formed molecules. A mechanism was proposed for the formation of cyclohexanone and a kinetic model was developed to predict the rate of cyclohexanone production as a function of light intensity and time. The photocatalytic experiments were performed according to a three-level full factorial design, which permitted (i) the calculation of kinetic parameters based on the genetic algorithm (GA) method and (ii) the model validation. To the best of our knowledge, no work on detailed kinetic evaluation of photocatalytic oxidation of cyclohexanol is available in the open literature.

2. Experimental

2.1. Materials

Cyclohexanol (99.0%), cyclohexanone (≥99.0%) and anatase TiO_2 (≥99.7%) were obtained from Sigma Aldrich. Hombikat UV-100 TiO_2 (100% anatase) was provided by Sachtleben Chemie GmbH and used as photocatalyst. TiO_2 Aeroxide P25 (≥99.5%) was provided by Evonik Industries. HPLC-grade acetonitrile (≥99.8%) was purchased from VWR.

2.2. TiO_2 film preparation

In order to choose the best TiO_2 for the film preparation, different TiO_2 samples such as Hombikat, P25, and Sigma-Aldrich anatase were first tested. It was found that only the Hombikat TiO_2 film was uniformly formed on the ZnSe ATR crystal and is thus suitable for *in situ* ATR–FTIR analysis. Therefore, the Hombikat sample with a surface area of 337 m^2/g and a primary particle size of approximately 5 nm was used to prepare a TiO_2 film for the *in situ* ATR–FTIR analysis [26]. Thin films of TiO_2 on ZnSe ATR crystals were prepared from a 3 g/L photocatalyst suspension. Suspensions were prepared using Milli-Q water. After ultrasonication for 30 min in a 35 kHz Elmasonic ultrasonic bath to to deagglomerate the TiO_2 particles, 1.5 mL of the prepared suspension was drop-casted on the crystal and dried overnight inside a vacuumed desiccator at ambient temperature.

2.3. In situ ATR–FTIR analysis

The transformation of cyclohexanol was analyzed using *in situ* ATR–FTIR spectroscopy. A VERTEX 70 Bruker FTIR spectrometer was employed for the spectroscopic analysis. A scheme of the employed setup is shown elsewhere [21]. The experiments were conducted using pure cyclohexanol instead of aqueous solutions to avoid the interference of cyclohexanol bands with intensive OH bands that appear in the presence of water. Prior to the start of each experiment, traces of water were removed from cyclohexanol overnight using a Molsieve (type 4A). Cyclohexanol was then oxygen saturated by purging with a 10 mL/min flow of dry air for 30 min. After depositing oxygen saturated cyclohexanol on the photocatalyst containing crystal (preparation described in Section 2.2), a spectrum was recorded at equilibrium adsorption and used as background. The photocatalytic transformation was initiated by irradiating 9×10^{-9} mol·(cm^2·s) of UV light with a wavelength centered at 375 nm. During illumination, one spectrum per minute was recorded from 700 to 4000 cm^{-1} with a resolution of 4 cm^{-1}. The spectra of background and photocatalytic reactions were averaged using 64 and 32 scans, respectively.

2.4. Photocatalytic experiments

The photocatalytic reactions for production of cyclohexanone were carried out in pyrex slurry- reaction cells. In each experiment, 10 mL of cyclohexanol and 1 g/L of TiO_2 photocatalyst were introduced into the cells and sonicated for 15 min to de-agglomerate the photocatalyst particles. Before starting irradiation, the cells were purged with pure oxygen for 15 min to ensure saturation of the suspension. The cells were stirred in the dark for 20 min for complete adsorption of cyclohexanol on the photocatalyst surface. Afterwards, the cells were irradiated with required number of 20 W Black-Ray® mercury tubes to provide 400, 800, or 1200 μW/cm^2 of light intensity. During the experiments, the cells were kept under 500 rpm magnetic stirring. A cooling fan was used to keep the temperature of the reaction cells around ambient during the reaction. The cells were radiated for 4, 7, and 10 days to transform cyclohexanol to cyclohexanone. At the end of experiment, 1 mL of suspension was filtered through a 0.45 μm Sarstedt syringe filtration unit into 1.5-mL vials and analyzed by HPLC to measure the amount of formed cyclohexanone. The experiments were repeated to ensure the accuracy of the results.

2.5. HPLC method

HPLC measurements were performed using a LC-30AD Shimadzu device equipped with a DGU-20A5 degasser, SIL-20A XR autosampler, and RID-10A detector. An Ultra C18 3 μm column (150 × 4.5 mm) with a mobile phase containing 50% acetonitrile in water was used for the analysis. In each analysis, 1 μL of sample was injected into the mobile phase with a 0.3 mL/min flow rate. LabSolutions software was used to analyze the data and calculate the amount of formed cyclohexanone. The actual concentration was calculated using appropriate calibration data.

2.6. Design of experiments

To evaluate the proposed model, photocatalytic experiments were designed based on the design of experiment approach [27]. These experiments were conducted according to a three-level full factorial design. Light intensity (μW/cm^2) and time (day) were defined as independent variables, labeled A and B (see Table 1). The range of independent variables was obtained based on preliminary experiments. The rate of cyclohexanone production was defined as the dependent variable (response). As demonstrated in Tables 1 and 2, nine sets of experiments were conducted in three levels and coded as −1, 0, and +1.

Table 1
Experimental ranges and levels of independent variables for photocatalytic experiments performed using slurry photoreactor.

Variables	−1	0	+1
Light intensity (A, μW/cm^2)	400	800	1200
Time (B, day)	4	7	10

Table 2
Values of independent variables obtained based on three-level full factorial design and corresponding rates of cyclohexanone production.

Run #	Independent variables		Rate of cyclohexanone production (mmol/day)	
	Light intensity (μW/ cm^2)	Time (day)	Experiment	Kinetic model
1	400	4	5.1	5.1
2	400	7	3.1	3.2
3	400	10	2.2	2.1
4	800	4	6.5	6.2
5	800	7	3.7	4.0
6	800	10	2.3	2.6
7	1200	4	7.0	7.0
8	1200	7	4.3	4.5
9	1200	10	3.2	2.9

2.7. Genetic algorithm (GA)

GA is a powerful method for solving optimization problems and takes advantage of a robust optimization procedure. It is inspired by the process of natural selection and its global optimizing capacity is more powerful than other heuristic optimization approaches [28]. In this work, the GA optimization method was used to determine the kinetic parameters. 200 individuals were selected and randomly distributed for each generation. Constraint dependent, rank, and stochastic uniform functions were selected as creation, fitness scaling, and selection functions, respectively. To generate new generations, 5% of the individuals were selected as elite count. Moreover, crossover and mutation were employed to generate respectively 80% and 20% of the subsequent generation. Constraint-dependent functions were considered for crossover and mutation.

2.8. Statistical analysis

The predicted rates of cyclohexanone production by the proposed kinetic model were statistically compared with the experimental values to evaluate the accuracy of the model. This statistical comparison was performed in terms of the coefficient of determination (R^2), adjusted coefficient of determination (R^2_{adj}), root mean squared error (*RMS*), mean absolute error (*MAE*), and absolute average deviation (*AAD*). In this regard, the following expressions were employed for the analysis:

$$R^2 = 1 - \sum_{i=1}^{n}\left(\frac{(y_{i,cal} - y_{i,\exp})^2}{(y_{ave,\exp} - y_{i,\exp})^2}\right) \quad (1)$$

$$R^2_{adj} = 1 - \left[(1 - R^2)\frac{n-1}{n-K-1}\right] \quad (2)$$

$$RMS = \sqrt{\frac{\sum_{i=1}^{n}(y_{i,cal} - y_{i,\exp})^2}{n}} \quad (3)$$

$$MAE = \frac{\sum_{i=1}^{n}|y_{i,cal} - y_{i,\exp}|}{n} \quad (4)$$

$$AAD = \left\{\frac{\sum_{i=1}^{n}(|y_{i,cal} - y_{i,\exp}|/y_{i,cal})}{n}\right\} \times 100 \quad (5)$$

where $y_{i,cal}$, $y_{i,\exp}$ and $y_{ave,\exp}$ are the predicted and experimental rates of cyclohexanone production, and the arithmetic mean of all of the experimental data, respectively. In addition, n and K represent the number of data points and independent variables. A better fit is achieved when R^2 is closer to 1, R^2_{adj} is closer to R^2, and *RMS, MAE,* and *AAD* are closer to zero.

3. Mechanistic and kinetic study

3.1. Mechanism of cyclohexanol conversion

A reaction mechanism was proposed for the production of cyclohexanone from cyclohexanol based on different steps, from charge separation to cyclohexanone molecule formation (k_i and K_i represent the reaction constant and equilibrium constant, respectively):

- Photocatalytic conversion of cyclohexanol to cyclohexanone initiates by the generation of an electron and hole pair as a result of absorbance of a photon of light by photocatalyst:

$$Photocatalyst + h\nu \xrightarrow{k_6} e^- + h^+ \quad (6)$$

- The photo-generated species tend to recombine rapidly and release heat [29]:

$$e^- + h^+ \xrightarrow{k_7} Heat \quad (7)$$

- The cyclohexanol molecule adsorbs on the active catalyst surface sites:

$$C_6H_{11} - OH + S \overset{K_8}{\leftrightarrows} C_6H_{11} - OH_{ads} \quad (8)$$

where S represents a free active reaction site.

- The photo-generated hole can be scavenged by the adsorbed cyclohexanol to release a proton.

$$C_6H_{11} - OH_{ads} + h^+ \xrightarrow{k_9} C_6H_{11} - O^{\cdot}_{ads} + H^+ \quad (9)$$

- The photo-generated electron can react with oxygen to generate a superoxide radical, as the liquid phase is saturated with oxygen:

$$O_2 + e^- \xrightarrow{k_{10}} O_2^- \quad (10)$$

- The photo-generated superoxide radical and proton react in a series of reactions according to Eqs. (11)–(15) to generate hydrogen peroxide [30]:

$$O_2^- + H^+ \xrightarrow{k_{11}} HO_2^{\cdot} \quad (11)$$

$$HO_2^{\cdot} + HO_2^{\cdot} \xrightarrow{k_{12}} H_2O_2 + O_2 \quad (12)$$

$$HO_2^{\cdot} + O_2^- \xrightarrow{k_{13}} HO_2^- + O_2 \quad (13)$$

$$HO_2^{\cdot} + e^- \xrightarrow{k_{14}} HO_2^- \quad (14)$$

$$HO_2^- + H^+ \xrightarrow{k_{15}} H_2O_2 \quad (15)$$

- The generated hydrogen peroxide converts to hydroxyl radical either by adsorption of a photon of light or reaction with a photo-generated electron:

$$H_2O_2 + h\nu \xrightarrow{k_{16}} 2^{\cdot}OH \quad (16)$$

$$H_2O_2 + e^- \xrightarrow{k_{17}} OH + OH^- \quad (17)$$

- Other than direct reaction of cyclohexanol with a photo-generated

hole (Eq. (9)), cyclohexanol can also react with hydroxyl radicals:

$$C_6H_{11}-OH_{ads}+OH \xrightarrow{k_{18}} C_6H_{11}-O^{\cdot}_{ads}+H_2O \quad (18)$$

- Finally, hydroxyl radical reacts with cyclohexanol radicals (generated either by reaction (9) or Eq. (18)) to produce cyclohexanone and water and re-establish the reaction site:

$$C_6H_{11}-O^{\cdot}_{ads}+OH \xrightarrow{k_{19}} C_6H_{10}=O+H_2O+S \quad (19)$$

In brief, based on the proposed mechanism, the cyclohexanol molecule releases two protons to produce cyclohexanone in two steps (reactions (9) and (19) or (18) and (19), depending on the path of the oxidation) and the generated protons indirectly react with the dissolved oxygen through Eqs. (10)–(17) to eventually form a water molecule (Eqs. (18) and/or (19)).

3.2. Kinetic model development

The kinetic model was developed based on the proposed mechanism (see Section 3.1). According to Eq. (19), the production rate of cyclohexanone (r_{Cnon}) can be calculated as:

$$r_{Cnon}=\frac{d[C_6H_{10}=O]}{dt}=k_{19}[C_6H_{11}-O^{\cdot}_{ads}][\cdot OH] \quad (20)$$

where [X] represents the concentration of X.

Assuming that the concentration of $C_6H_{11}-O^{\cdot}_{ads}$ radicals is constant during the reaction, the variation rate of $[C_6H_{11}-O^{\cdot}_{ads}]$ is zero:

$$\frac{dC_{C_6H_{11}-O^{\cdot}}}{dt}=k_9[C_6H_{11}-OH_{ads}][h^+]+k_{18}[C_6H_{11}-OH_{ads}][\cdot OH]-k_{19}[C_6H_{11}-O^{\cdot}_{ads}][\cdot OH]=0 \quad (21)$$

Accordingly, $[C_6H_{11}-O^{\cdot}_{ads}]$ can be calculated as follows:

$$[C_6H_{11}-O^{\cdot}_{ads}]=\frac{(k_9[h^+]+k_{18}[\cdot OH])[C_6H_{11}-OH_{ads}]}{k_{19}[\cdot OH]} \quad (22)$$

By considering that the rate of direct photocatalytic conversion of cyclohexanol (reaction with photogenerated holes) is much higher than the rate of its indirect photocatalytic conversion (reaction with $^{\cdot}OH$ radicals generated in the photocatalytic process) [31], Eq. (22) can be simplified to Eq. (23):

$$[C_6H_{11}-O^{\cdot}_{ads}]=\frac{k_9[h^+][C_6H_{11}-OH_{ads}]}{k_{19}[\cdot OH]} \quad (23)$$

The concentration of adsorbed cyclohexanol can be determined based on Eq. (8) as follows:

$$[C_6H_{11}-OH_{ads}]=K_8[C_6H_{11}-OH][S] \quad (24)$$

where [S] represents the concentration of reaction sites and K_8 is the equilibrium constant of Eq. (8). The total concentration of reaction sites is constant during the reaction and can be defined as:

$$[S_0]=[S_{act}]+[S_{dec}] \quad (25)$$

where $[S_{act}]$ and $[S_{dec}]$ correspond to the active and deactivated reaction sites, respectively. The active reaction sites are composed of free sites and sites occupied by cyclohexanol.

$$[S_{act}]=[S]+[C_6H_{11}-OH_{ads}] \quad (26)$$

The active reaction sites deactivate according to Eq. (27). By assuming the deactivation as a first order reaction, the concentration of active reaction sites can be expressed by Eq. (28):

$$[S_{act}]\rightarrow[S_{dec}] \quad (27)$$

$$[S_{dec}]=[S_0]\times(1-\exp(-k_{dec}t)) \quad (28)$$

where k_{dec} represents the first-order rate constant of active site deactivation and t is the reaction time. As the number of reaction sites depends on the catalyst concentration in the reaction media, $[S_0]$ is a function of catalyst loading:

$$[S_0]=a[Cat]^b \quad (29)$$

where [*Cat*] represents the catalyst loading and a and b are constants. b should be equal or lower than 1 to take into account the possible agglomeration of catalyst [7].

The concentration of free reaction sites can be obtained by substituting Eqs. (24), (26), (28), (29) in Eq. (25) as follows:

$$[S]=\frac{a[Cat]^b\exp(-k_{dec}t)}{1+K_8[C_6H_{11}-OH]} \quad (30)$$

The rate of reaction (6) is a function of catalyst loading and light intensity [32,33]:

$$r_1=k_6[Cat]^q(\phi I)^l \quad (31)$$

where q and l are constants and φ is quantum efficiency. q and l are the orders of reaction with respect to the catalyst load and light intensity, respectively.

The rate of the reaction (7) can be expressed by Eq. (32), considering the equality between the concentrations of photo-generated (i) electrons and (ii) holes [34]:

$$r_2=k_7[h^+]^2 \quad (32)$$

The concentration of photo-generated holes can be considered as constant [34], as a result:

$$\frac{d[h^+]}{dt}=k_6[Cat]^q(\phi I)^l-k_7[h^+]^2-k_9[h^+][C_6H_{11}-OH]=0 \quad (33)$$

As the rate of photogenerated species recombination is very fast [34,35], by assuming $k_7[h^+]^2>>k_9[h^+][C_6H_{11}-OH]$, the concentration of photo-generated holes can be calculated as follows:

$$[h^+]=\sqrt{\frac{k_6[Cat]^q(\phi I)^l}{k_7}} \quad (34)$$

By substituting Eqs. (23), (24), (30), and (34) in Eq. (20), the rate of cyclohexanone production can be obtained as follows:

$$r_{Cnon}=\alpha I^{\beta}\exp(\gamma t) \quad (35)$$

where $\alpha=\frac{a\sqrt{k_6/k_7}k_9K_8\phi^{l/2}[C_6H_{11}-OH][Cat]^{b+q/2}}{1+K_8[C_6H_{11}-OH]}$, $\beta=l/2$, and $\gamma=-k_{dec}$. Eq. (35) determines the rate of cyclohexanone production as a function of light intensity and time, and this rate equation can be easily used in practice. In Eq. (35), I^{β} is the term related to the effect of light intensity (β is the pseudo-exponent of light intensity). It shows that the rate of cyclohexanone production increases as a power function with respect to the light intensity. The term $\exp(\gamma t)$ is related to the deactivation of photocatalyst, where γ depends on the first-order rate constant of the active surface sites deactivation (k_{dec}, Eq. (28)).

4. Results

4.1. ATR–FTIR analysis

ATR–FTIR analysis during the photocatalytic reaction was performed to *experimentally investigate the cyclohexanone production and confirm the proposed reaction mechanism.* The obtained spectra in the wavenumber range between 1000 and 4000 cm^{-1} for the time range of 0–200 min are depicted in Fig. 1a. The spectra of adsorbed cyclohexanol on the TiO_2 surface (in dark condition) were considered as reference for this measurement. To find the IR bands of cyclohexanol and cyclohexanone, ATR–FTIR measurements were performed using pure cyclohexanol and 1% dissolved cyclohexanone in cyclohexanol in the absence of light (Fig. 1b). According to Fig. 1b, the main cyclohexanol bands are located at 1030, 1065, 1366, 1449, 2855, and 2929 cm^{-1}. An obvious indicative band of cyclohexanone is positioned at 1713 cm^{-1}, which is attributed to the C=O stretching vibration of cyclohexanone. As can be seen in Fig. 1a, negative bands related to cyclohexanol

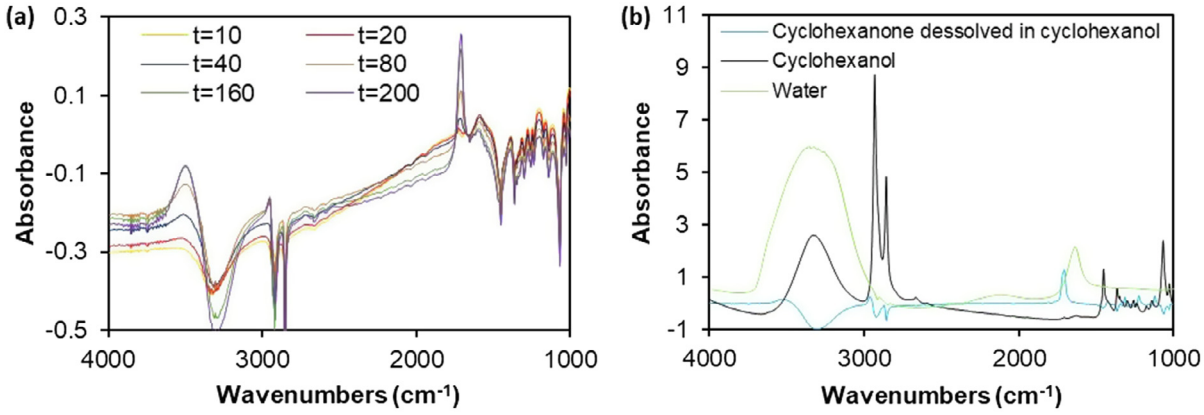

Fig. 1. ATR–FTIR spectra of (a) cyclohexanol photooxidation in the range of 1000 and 4000 cm^{-1} for 200 min of reaction time, (b) spectra of respectively 1% cyclohexanone dissolved in cyclohexanol, cyclohexanol, and water.

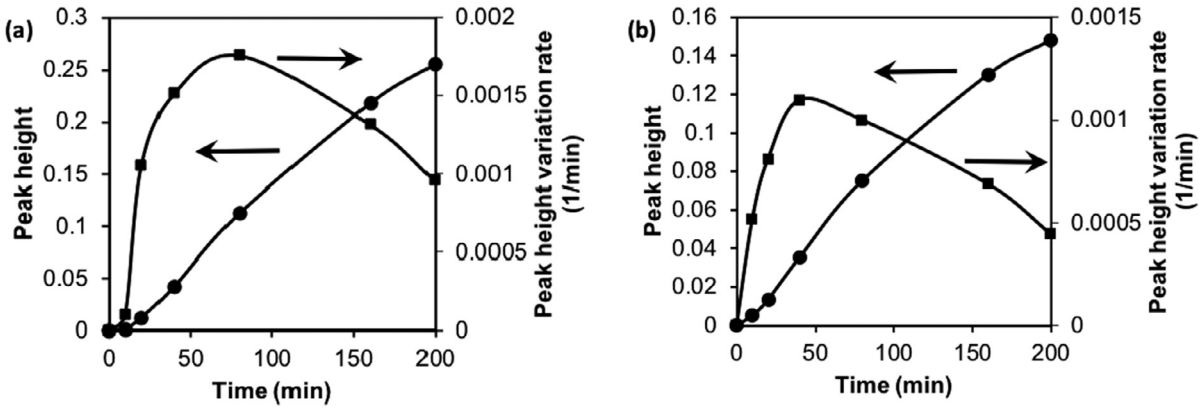

Fig. 2. Time profiles of product formation obtained from peak deconvolution at (a) 1713 cm^{-1} (cyclohexanone) and (b) 3390 cm^{-1} (water).

Table 3
The values of kinetic parameters of the proposed kinetic model.

Kinetic parameter	Value
α	1.521
β	0.2994
γ	−0.1482

appeared during illumination, representing cyclohexanol transformation. In addition, two positive bands appeared at 1713 and 3390 cm^{-1}. The band at 1713 cm^{-1} is attributed to cyclohexanone (as suggested by Fig. 1b) and confirms the transformation of cyclohexanol to cyclohexanone during the photocatalytic reaction. In addition, the observed band at 3390 cm^{-1} is related to OH stretching vibrations of water (as suggested by Fig. 1b). These results confirm the accuracy of the proposed mechanism in which cyclohexanol is directly converted into cyclohexanone and water (no intermediates were detected), cf. to the Eqs. (18) and (19).

In addition, the heights of the bands observed at 1713 and 3390 cm^{-1} were analyzed and the results are presented in Fig. 2a and b, respectively. The height of the bands increases continuously, demonstrating continuous formation of cyclohexanone and water. In both cases, a maximum in the production rate can be observed. Compared to cyclohexanone formation, the maximum rate of water formation occurred at earlier times, suggesting that the desorption of water from the catalyst surface occurred prior to cyclohexanone desorption (Eq. (19)). Interestingly, bands that could be assigned to deactivating species such as carbonates and carboxylates, which are abundant in experiments where cyclohexane is oxidized [36], did not develop significantly,

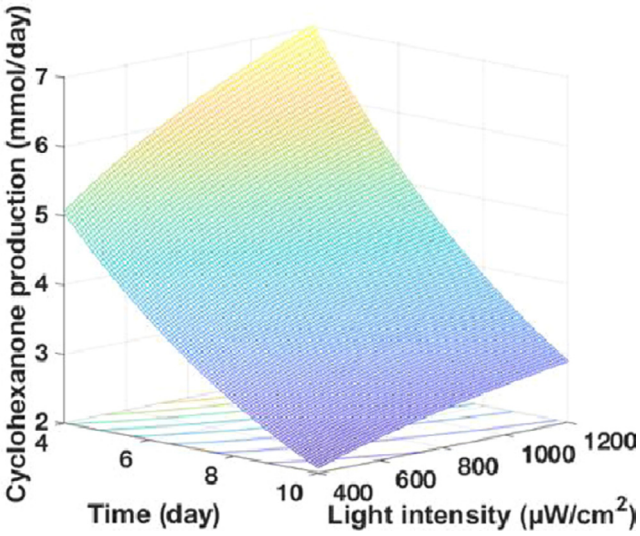

Fig. 3. Three dimensional model prediction of the cyclohexanone production rate as a function of light intensity and time.

suggesting that the catalyst surface is less sensitive to deactivation during oxidation of cyclohexanol as compared to oxidation of cyclohexane. This may be attributed to the fact that cyclohexanol oxidation to cyclohexanone can occur in two steps (reactions (9) and (19) or (18) and (19)). However, the formation of a double bond between oxygen and cyclohexane (for cyclohexanone generation) is a complex process that occurs in several steps, thus increasing the chances of the

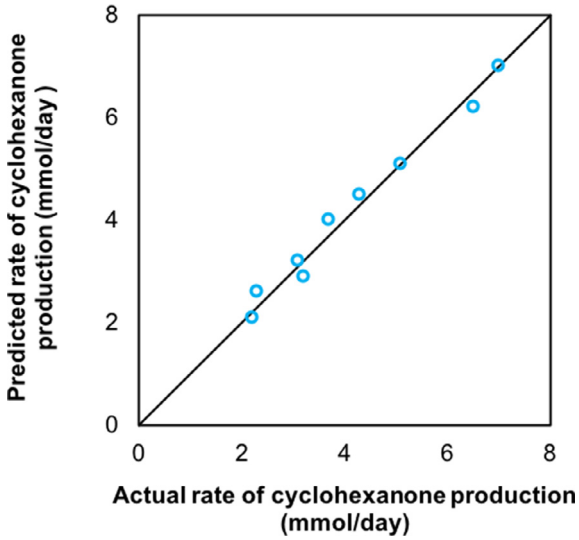

Fig. 4. Comparison between the kinetic model predictions of cyclohexanone production rate with the obtained experimental results.

Table 4
Statistical comparison between the kinetic model predictions and experimental data.

Parameter	Value
R^2	0.9825
$R^2_{adj.}$	0.9537
RMS	0.2160
AAD	0.7927
MAE	0.0267

formation of deactivating species as side products [37].

4.2. Evaluation of the proposed kinetic model accuracy

To *evaluate the accuracy of the proposed kinetic model*, photocatalytic experiments were performed in a slurry photoreactor based on three-level full factorial experimental design. The rate of cyclohexanone production was measured by HPLC analysis of the products and the results are presented in Table 2. It is worth mentioning that the detection of cyclohexanone as final product was also verified by GC–MS (data not shown here). In agreement with the spectroscopic data, an excellent (almost 100%) selectivity of cyclohexanone (H_2O free basis) was confirmed.

The kinetic parameters of Eq. (35) (Table 3) were calculated based on the experimental data (Table 2) and GA (as described in Section 2.7). For this purpose, the experimental values of cyclohexanol production rate obtained at different light intensities and times (Table 2) were substituted into Eq. (35) and the kinetic parameters (α, β, and γ) were then estimated using a MATLAB code, prepared based on the described GA method. Based on the values of β (0.2993) and γ (−0.1482), the order of reaction (6) with respect to the light intensity, I, is equal to 0.5986 ($\beta = I/2$) and the constant of site deactivation (k_{dec}) is 0.1482 ($\gamma = -k_{dec}$).

Fig. 3 presents a three-dimensional graphical representation of the model predictions as a function of light intensity and time. It was observed that the rate of cyclohexanone production enhances by increasing the intensity of light, but decreases as a function of time. Fig. 4 (diagram of dispersion) and Table 4 (parameters of the statistical analysis, as described in Section 2.8) show the very good agreement between the predicted cyclohexanone production rates and experimental data. Data from Table 4 (R^2 close to 1, R^2_{adj} close to R^2, and *RMS*, *AAD*, and *MAE* close to zero) demonstrate the capability of the proposed model to predict the rate of cyclohexanone formation very well. Accordingly, Fig. 4 and Table 4 confirm that the effects of light intensity and time can be modeled as power and exponential functions with a high accuracy. Modeling of the effect of light intensity and time is of high interest because these two parameters are known as the most effective in photocatalytic reactions [38,39].

These results demonstrate that photocatalysis can be a promising technology for the production of cyclohexanone from cyclohexanol, not only for the excellent selectivity of cyclohexanone, but because of a low catalyst deactivation in comparison to cyclohexane conversion to cyclohexanone, due to avoiding the formation of significant amounts of carbonates and carboxylates. Nevertheless, further extensive work still needs to be done to enhance the rate of reaction, for eventual industrial implementation of this technology.

5. Conclusion

In this work, spectroscopic and kinetic studies were performed on the photocatalytic cyclohexanone production from cyclohexanol. *In situ ATR-FTIR* analysis of the photocatalytic reaction was employed to investigate this process, and revealed that the oxidation of surface bound cyclohexanol is highly selective without the formation of significant amounts of carbonates and carboxylates. A kinetic model was then developed (based on the present mechanism) to predict the rate of cyclohexanone production. The comparison between the experimental data and the kinetic model developed showed that the effects of light intensity and time can be modeled as power and exponential functions, respectively. Both spectroscopic and chromatographic analyses demonstrated an excellent selectivity of cyclohexanone, and it proved that the photocatalytic approach could be a promising alternative for production of cyclohexanone from cyclohexanol.

Acknowledgements

The authors are very grateful to the Ministry of Education and Higher Education of Quebec, Fonds de recherche du Québec Nature et technologies (FRQNT), Natural Sciences and Engineering Research Council of Canada (NSERC), TELUS, and Laval University for financial support and Ph.D. scholarships for M.R. Karimi Estahbanati.

References

[1] T. Zadi, A.A. Assadi, N. Nasrallah, R. Bouallouche, P.N. Tri, A. Bouzaza, M.M. Azizi, R. Maachi, D. Wolbert, Treatment of hospital indoor air by a hybrid system of combined plasma with photocatalysis: case of trichloromethane, Chem. Eng. J. 349 (2018) 276–286.
[2] Y. Sheng, Z. Wei, H. Miao, W. Yao, H. Li, Y. Zhu, Enhanced organic pollutant photodegradation via adsorption/photocatalysis synergy using a 3D g-C_3N_4/TiO_2 free-separation photocatalyst, Chem. Eng. J. 287–294 (2019).
[3] M. Feilizadeh, M. Vossoughi, S.M.E. Zakeri, M. Rahimi, Enhancement of efficient Ag–S/TiO_2 nanophotocatalyst for photocatalytic degradation under visible light, Ind. Eng. Chem. Res. 53 (2014) 9578–9586.
[4] Y. Boyjoo, H. Sun, J. Liu, V.K. Pareek, S. Wang, A review on photocatalysis for air treatment: from catalyst development to reactor design, Chem. Eng. J. 310 (2017) 537–559.
[5] X. Hu, X. Hu, Q. Peng, L. Zhou, X. Tan, L. Jiang, C. Tang, H. Wang, S. Liu, Y. Wang, Mechanisms underlying the photocatalytic degradation pathway of ciprofloxacin with heterogeneous TiO_2, Chem. Eng. J. (2019), https://doi.org/10.1016/j.cej.2019.122366.
[6] Z. Liu, Y. Zhang, L. Kong, L. Liu, J. Luo, B. Liu, Q. Zhou, F. He, D. Xu, Z. Wu, Preparation and preferential photocatalytic degradation of acephate by using the composite photocatalyst Sr/TiO_2-PCFM, Chem. Eng. J. (2019).
[7] M.R. Karimi Estahbanati, M. Feilizadeh, M.C. Iliuta, Photocatalytic valorization of glycerol to hydrogen: optimization of operating parameters by artificial neural network, Appl. Catal. B: Environ. 209 (2017) 483–492.
[8] Q. Li, Y. Xia, C. Yang, K. Lv, M. Lei, M. Li, Building a direct Z-scheme heterojunction photocatalyst by $ZnIn_2S_4$ nanosheets and TiO_2 hollowspheres for highly-efficient artificial photosynthesis, Chem. Eng. J. 349 (2018) 287–296.
[9] M.R. Karimi Estahbanati, M. Feilizadeh, M. Shokrollahi Yancheshmeh, M.C. Iliuta, Effects of carbon nanotube and carbon sphere templates in TiO_2 composites for photocatalytic hydrogen production, Ind. Eng. Chem. Res. 58 (2019) 2770–2783.
[10] S. Zhu, W. Liao, M. Zhang, S. Liang, Design of spatially separated Au and CoO dual cocatalysts on hollow TiO_2 for enhanced photocatalytic activity towards the

reduction of CO_2 to CH_4, Chem. Eng. J. 361 (2019) 461–469.
[11] V.M. Daskalaki, P. Panagiotopoulou, D.I. Kondarides, Production of peroxide species in Pt/TiO_2 suspensions under conditions of photocatalytic water splitting and glycerol photoreforming, Chem. Eng. J. 170 (2011) 433–439.
[12] J. Huang, Y. Cao, H. Wang, H. Yu, F. Peng, H. Zou, Z. Liu, Revealing active-site structure of porous nitrogen-defected carbon nitride for highly effective photocatalytic hydrogen evolution, Chem. Eng. J. 373 (2019) 687–699.
[13] A. Maldotti, A. Molinari, R. Amadelli, Photocatalysis with organized systems for the oxofunctionalization of hydrocarbons by O_2, Chem. Rev. 102 (2002) 3811–3836.
[14] Y. Zhang, R. Ciriminna, G. Palmisano, Y.-J. Xu, M. Pagliaro, Sol-gel entrapped visible light photocatalysts for selective conversions, RSC Adv. 4 (2014) 18341–18346.
[15] J. Ritz, H. Fuchs, H. Kieczka, W.C. Moran, "Caprolacatam" in Ullmann's Encyclopedia of Industrial Chemis, Wiley VCH, Weinheim, Germany, 2005.
[16] W.B. Fisher, J.F. VanPeppen, Cyclohexanol and Cyclohexanone, Kirk-Othmer Encyclopedia of Chemical Technology, (2000).
[17] W.B. Fisher, J.F. Van Pepper, M. Grayson, Kirk-Othner Encyclopedia of Chemical Technology, third ed., Wiley, New York, 1979.
[18] Y.-X. Yu, X. Ying, T.-J. Wang, Q. Zhang, X.-H. Zhang, X. Zhang, In-situ hydrogenation of lignin depolymerization model compounds to cyclohexanol, J. Fuel Chem. Technol. 41 (2013) 443–447.
[19] P. Anastas, N. Eghbali, Green chemistry: principles and practice, Chem. Soc. Rev. 39 (2010) 301–312.
[20] M.D. Hernández-Alonso, A.R. Almeida, J.A. Moulijn, G. Mul, Identification of the role of surface acidity in the deactivation of TiO_2 in the selective photo-oxidation of cyclohexane, Catal. Today 143 (2009) 326–333.
[21] A.R. Almeida, J.A. Moulijn, G. Mul, In situ ATR-FTIR study on the selective photo-oxidation of cyclohexane over anatase TiO_2, Phys. Chem. C 112 (2008) 1552–1561.
[22] J. Kou, C. Lu, J. Wang, Y. Chen, Z. Xu, R.S. Varma, Selectivity enhancement in heterogeneous photocatalytic transformations, Chem. Rev. 117 (2017) 1445–1514.
[23] F. Parrino, M. Bellardita, E.I. García-López, G. Marcì, V. Loddo, L. Palmisano, Heterogeneous photocatalysis for selective formation of high-value-added molecules: Some chemical and engineering aspects, ACS Catal. 8 (2018) 11191–11225.
[24] O.S. Mohamed, S.A. Ahmed, M.F. Mostafa, A.-M.A. Abdel-Wahab, Nanoparticles-photocatalytic oxidation of selected cycloalkanols, Int. J. Photoenergy 2008 (2008) 1–11, https://doi.org/10.1155/2008/205358.
[25] B. Srinivas, K. Lalitha, P.A.K. Reddy, G. Rajesh, V.D. Kumari, M. Subrahmanyam, B.R. De, Cyclohexanol dehydrogenation over Cu-loaded TiO_2 photocatalyst under solar illumination, Res. Chem. Intermed. 37 (2011) 1069–1086.
[26] P. Du, J.A. Moulijn, G. Mul, Selective photo (catalytic)-oxidation of cyclohexane: effect of wavelength and TiO_2 structure on product yields, J. Catal. 238 (2006) 342–352.
[27] M. Feilizadeh, I. Alemzadeh, A. Delparish, M.R. Karimi Estahbanati, M. Soleimani, Y. Jangjou, A. Vosoughi, Optimization of operating parameters for efficient photocatalytic inactivation of Escherichia coli based on a statistical design of experiments, Water Sci. Technol. 71 (2015) 823–831.
[28] B. Saha, P. Chowdhury, A.K. Ghoshal, Al-MCM-41 catalyzed decomposition of polypropylene and hybrid genetic algorithm for kinetics analysis, Appl. Catal. B: Environ. 83 (2008) 265–276.
[29] H. Park, H.-I. Kim, G.-H. Moon, W. Choi, Photoinduced charge transfer processes in solar photocatalysis based on modified TiO_2, Energy Environ. Sci. 9 (2016) 411–433.
[30] J. Chen, D.F. Ollis, W.H. Rulkens, H. Bruning, Photocatalyzed oxidation of alcohols and organochlorides in the presence of native TiO_2 and metallized TiO_2 suspensions. Part (II): photocatalytic mechanisms, Water Res. 33 (1999) 669–676.
[31] A.R. Amani-Ghadim, M.S.S. Dorraji, Modeling of photocatalyatic process on synthesized ZnO nanoparticles: kinetic model development and artificial neural networks, Appl. Catal. B: Environ. 163 (2015) 539–546.
[32] T. Hisatomi, T. Minegishi, K. Domen, Kinetic assessment and numerical modeling of photocatalytic water splitting toward efficient solar hydrogen production, Bull. Chem. Soc. Jpn. 85 (2012) 647–655.
[33] M.R. Karimi Estahbanati, M. Feilizadeh, M.C. Iliuta, An intrinsic kinetic model for liquid phase photocatalytic hydrogen production, AIChE J. (2019), https://doi.org/10.1002/aic.16724.
[34] M. Fathinia, A. Khataee, S. Aber, A. Naseri, Development of kinetic models for photocatalytic ozonation of phenazopyridine on TiO_2 nanoparticles thin film in a mixed semi-batch photoreactor, Appl. Catal. B: Environ. 184 (2016) 270–284.
[35] D.W. Bahnemann, M. Hilgendorff, R. Memming, Charge carrier dynamics at TiO_2 particles: reactivity of free and trapped holes, Phys. Chem. B 101 (1997) 4265–4275.
[36] J.T. Carneiro, T.J. Savenije, J.A. Moulijn, G. Mul, The effect of Au on TiO_2 catalyzed selective photocatalytic oxidation of cyclohexane, J. Photochem. Photobiol. A 217 (2011) 326–332.
[37] P. Boarini, V. Carassiti, A. Maldotti, R. Amadelli, Photocatalytic oxygenation of cyclohexane on titanium dioxide suspensions: effect of the solvent and of oxygen, Langmuir 14 (1998) 2080–2085.
[38] A.V. Puga, Photocatalytic production of hydrogen from biomass-derived feedstocks, Coord. Cem. Rev. 315 (2016) 1–66.
[39] T. Jedsukontorn, V. Meeyoo, N. Saito, M. Hunsom, Route of glycerol conversion and product generation via TiO_2-induced photocatalytic oxidation in the presence of H_2O_2, Chem. Eng. J. 281 (2015) 252–264.